ADVANCED FUNCTIONAL MATERIALS
www.afm-journal.de

Formation of Spherical and Non-Spherical Eutectic Gallium-Indium Liquid-Metal Microdroplets in Microfluidic Channels at Room Temperature

Tanya Hutter, Wolfgang-Andreas C. Bauer, Stephen R. Elliott, and Wilhelm T. S. Huck**

Here, the formation of eutectic Gallium-Indium (EGaIn) liquid-metal microdroplets, both spherical and non-spherical, in microfluidic devices at room temperature is reported. Monodisperse microdroplets were created in an aqueous polyethylene glycol (PEG) solution, in oxygenated and in deoxygenated silicone oil. The volume of the droplets depends on the channel dimensions and flow rates applied, varying between 0.5 and 4 nL. Non-spherical droplets were formed in oxygenated silicone oil due to the instantaneous formation of an oxide layer. These metal "micro-rice" droplets retained their shape and did not spontaneously reflow to form shapes of the lowest interfacial energy on egress from the channel, unlike in aqueous PEG solution and in deoxygenated silicone oil. Liquid-metal droplets with such tunable morphology can potentially be used in MEMS devices for optical and electrical switches, valves and micropumps.

1. Introduction

Microdroplets in microfluidics have become a highly interesting platform in various research areas, such as chemistry, biochemistry, molecular biology, and materials science.[1–3] A key advantage of droplet-based microfluidic systems over conventional bulk emulsification techniques is the possibility to produce monodisperse microdroplets with a wide range of accessible volumes (typically fL to nL).[4] Moreover, the microfluidic approach allows for high-throughput droplet generation at frequencies of the order of tens of kHz,[5] as well as for the integration of functional modules enabling precise modes of droplet manipulation on-chip, e.g., droplet fusion,[6,7] splitting[8] and sorting.[9] It has also been demonstrated that microdroplet technology can easily be combined with a range of analytical methods, such as mass spectrometry,[10] fluorescence detection[11] or optical tweezers.[12]

T. Hutter, W.-A. C. Bauer, Prof. S. R. Elliott, Prof. W. T. S. Huck
Department of Chemistry
University of Cambridge
Lensfield Road, Cambridge, CB2 1EW, U.K.
E-mail: sre1@cam.ac.uk
Prof. W. T. S. Huck
Radboud University Nijmegen
Institute for Molecules and Materials
Heyendaalseweg 135, Nijmegen, 6525 AJ, The Netherlands
E-mail: w.huck@science.ru.nl

DOI: 10.1002/adfm.201200324

Mercury droplets have been used in microchannels as electrodes for electrochemistry,[13] where the liquid mercury adopts a shape that minimizes its surface energy. Recently, the fabrication and characterization of liquid-metal microfluidic electrodes, where the channels define the shape and position of the aligned microelectrodes, have been described.[14] Polydimethyl siloxane (PDMS) is able to withstand temperatures up to 400 °C for limited times[15] and therefore it is possible to inject molten metals and alloys (e.g., In, Sn, Ga, In/Sn, In/Ag, Ga/In) into PDMS microfluidic channels by heating the metals and channels, and allowing the metal to solidify therein on cooling.[16] Production of Bi alloy particles in microfluidic channels was reported.[17] The authors formed liquid-metal droplets at a temperature that is above the liquid–solid phase transition of the alloy, and then cooled the outlet channel to a lower temperature to solidify the droplets.

Alloys based on gallium and indium are used as heat-transfer agents, as lubricating materials and low-temperature solders. In microfluidics, such non-toxic liquid metals have been reported to be used as electrodes. Eutectic Gallium-Indium (EGaIn) is a low-viscosity liquid above 15.3 °C, with a composition of 75.5% Ga and 24.5% In by weight. EGaIn has low toxicity, low electrical resistivity, low viscosity and low vapor pressure. It has been shown that EGaIn can readily flow and fill microchannels.[18] According to previous studies,[14,18–20] gallium-based alloys easily oxidize in air at room temperature to form a thin Ga_2O_3 'skin', which helps to stabilize mechanically the alloy within the microchannels. The skin is so thin that it does not alter significantly the electrical properties of the alloy.[19] In order to be able to flow the metal into a channel, the applied pressure at the inlet has to exceed the critical pressure required to rupture the skin.[18] The smaller the cross-sectional dimensions of the channel, the higher the critical pressure. The oxide skin is also responsible for the production of stable free-standing structures in which the surface energy is not minimized, as in normal liquids, and thus various shapes can be created.[19]

Different devices based on metals in microfluidics have been reported: a hyperelastic pressure transducer has been fabricated by embedding silicone rubber with microchannels of conductive liquid EGaIn.[21] Microfluidic channels of

a particular shape and filled with mercury have been used to make a reconfigurable electromagnetic metamaterial operating at microwave wavelengths.[22] There is a growing demand for stretchable antennas for implantable medical devices, remote sensing, interactive gaming and body-worn deformable devices. High-performance stretchable antennas have been fabricated, based on liquid-metal Galinstan (a eutectic alloy of Ga, In and Sn) filling microstructured channels in an elastic dielectric material.[23–25] Elastic liquid-metal antennas based on a eutectic gallium and indium alloy have been fabricated.[26,27] Microdroplets have the unique features of uniformity, periodicity and self-assembly that make them suitable for optics. Microfluidic droplets have been utilized in optics as reconfigurable optical diffraction gratings.[28,29]

Another important application of liquid metal-droplets is in continuous electrowetting (CEW) devices, where single liquid-metal droplets are placed in a capillary or microfluidic channel and driven in an electrolyte-filled capillary by locally modifying the surface tension with a varying electric potential.[30] This technique can be applied to fabricate optical switches, micropumps and microvalves for microelectromechanical systems (MEMS) devices, and it has very important advantages, including low driving voltage, high speeds and smooth operation without friction and wear.[31] An ultra-high contrast light valve was fabricated with liquid gallium displaying a very high contrast ratio and fast response time.[32] The problem has been that it is difficult to build such devices with a single repeatable liquid-metal droplet inside a microchannel. Various methods have been proposed to solve this problem;[33,34] however they are time consuming and complicated. Producing metallic microdroplets in microfluidic channels, and then manipulating them into desired locations, would therefore open the way forward to produce reproducible devices compatible with mass production.

Here we report on the formation of EGaIn liquid-metal microdroplets in microfluidic channels at room temperature. The droplet formation has been studied for different kinds of carrier liquids and various flow rates. The compatibility of surfactants to stabilize the formed liquid-metal droplets is demonstrated. Interestingly, under certain circumstances, the formed microdroplets do not spontaneously coalesce but retain their shape. Therefore, under such conditions, there is no need to add any surfactants and non-spherical geometries can be preserved. We show that the channel dimensions are critical in forming the shape of the microdroplets; wider channels favor spherical microdroplets, while narrower channels produce rod-like drops with an aspect ratio of ~2 ("micro-rice").

2. Results and Discussion

2.1. Droplet Formation in Aqueous PEG Solution

In a first series of liquid-metal droplets formation experiments, we used water containing 20 wt% poly(ethylene glycol) (PEG) and 5 wt% sodium dodecylsulfate (SDS) as the continuous phase at volumetric flow rates of $200 \leq Q_c \leq 900$ μL h^{-1}. PEG was used in order to create a high-viscosity fluid. The use of SDS was necessary, as omitting the surfactant caused large-scale coalescence of produced droplets when extruding them through a piece of tubing into the storage beaker. As the dispersed droplet phase, we introduced EGaIn at flow rates of $100 \leq Q_d \leq 800$ μL h^{-1}. Keeping the total flow rate ($Q_c + Q_d$) at a constant value of 1000 μL h^{-1}, we systematically varied the flow-rate ratio (Q_c/Q_d) between 0.25 and 9. For the production of liquid-metal microdroplets, we used PDMS-based microfluidic devices exhibiting a simple flow-focusing geometry, with either a 40 μm or 80 μm cross-section at the narrowest part of the nozzle (Supporting Information, Figure S1 and Figure S2, respectively). In order to adjust the channel surface properties to the aqueous continuous phase, we deposited a hydrophilic polyelectrolyte multilayer onto the channel wall prior to experiments, as described elsewhere.[35] The liquid-metal droplet formation process was monitored on-chip via a high-speed camera attached to an optical microscope.

2.1.1. Droplet Formation in 40 μm Flow-Focusing Devices

Microscopy images obtained from movies recorded at different flow-rate ratios using the 40 μm nozzle geometry are shown in **Figure 1a**. Based on these movies (Supporting Information, Movie M1) taken at a constant frame rate of 2400 pictures per second, we calculated droplet-formation frequencies for each Q_c/Q_d value. Moreover, droplet volumes were obtained by dividing the volumetric flow rate Q_d by the formation frequency. Both frequencies and droplet volumes are plotted against Q_c/Q_d in Figure 1b. With increasing flow-rate ratios from $Q_c/Q_d = 0.25$ to $Q_c/Q_d = 9$, i.e., with decreasing relative flow rates of the liquid metal, droplet volumes exhibit a sharp drop from 1.6 nL to 0.25 nL, respectively, which is confirmed by comparing the microscopy images in Figure 1. In contrast, with increasing flow-rate ratios, the droplet-formation frequency rises from 138 Hz at $Q_c/Q_d = 0.25$ to its maximum of 276 at $Q_c/Q_d = 1$ before it gradually decreases to 112 at $Q_c/Q_d = 9$. This behavior can be explained by the fact that the decline in droplet volume with increasing Q_c/Q_d promotes the formation frequency, whereas the reduction of the relative liquid-metal flow rate works in the opposite direction. Due to the steepness of the volume curve at low flow-rate ratios ($Q_c/Q_d < 1$), the formation frequency is dominated by the stimulating volume effect. As the volume curve flattens with increasing flow-rate ratio, the frequency becomes dominated by the inhibitive flow-rate effect for $Q_c/Q_d > 1$.

At a flow-rate ratio of 3, we collected the liquid-metal droplets in aqueous PEG solution in a reservoir (Figure 1c). It can be seen that the droplets are stable and do not coalesce. The histogram displaying the diameter distribution of the droplets is shown in Figure 1d. It was determined by fitting circles to 100 droplets (ImageJ software); based on the area values (in square pixels), the droplet diameters (in pixels) were calculated, which were then converted into diameters (in μm) using a microscope scale bar. The average droplet diameter was found to be 83 (± 0.7) μm. The standard deviation being below 1% of the mean diameter proves that the EGaIn microdroplets are truly monodisperse.

2.1.2. Droplet Formation in 80 μm Flow-Focusing Devices

The liquid-metal droplet formation at different flow-rate ratios in the microfluidic chip using the 80 μm nozzle size is shown

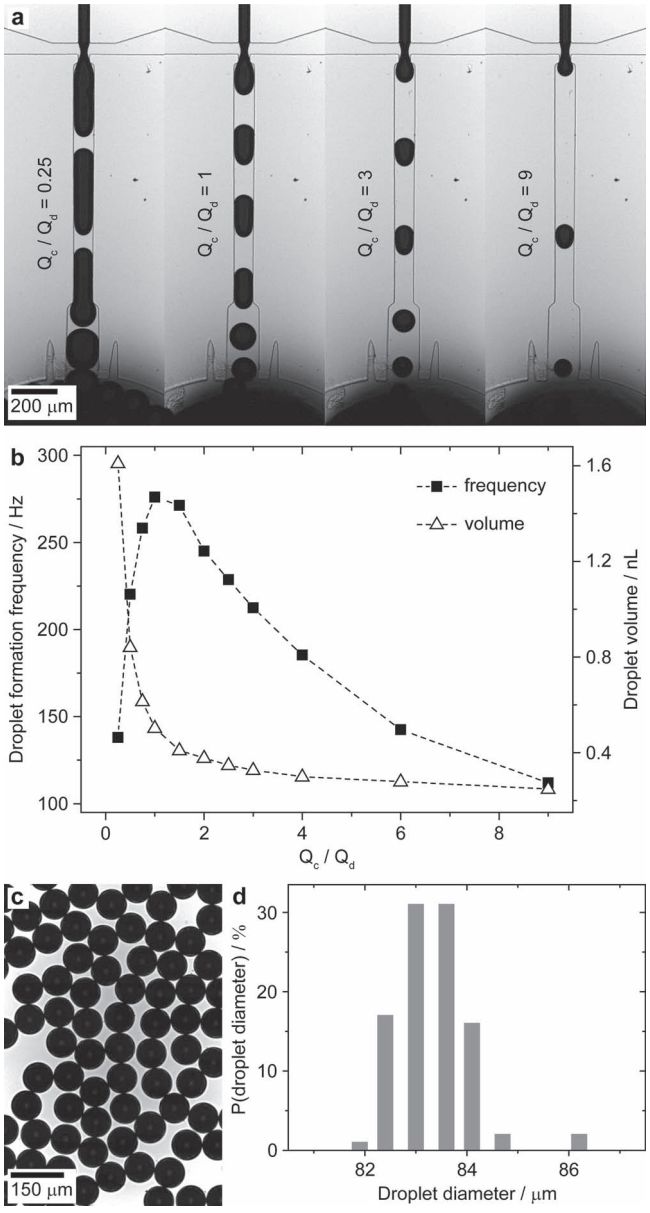

Figure 1. Liquid-metal droplet formation in aqueous PEG solution using a device with 40 µm nozzle geometry. a) Series of microscopy images depicting the droplet generation at different flow- rate ratios. b) Formation frequency and volume of liquid-metal droplets vs. flow-rate ratio Q_c/Q_d. c) Microscopy image showing a sample of liquid-metal droplets produced at Q_c/Q_d = 3 inside a reservoir. d) Droplet diameter distribution of the sample.

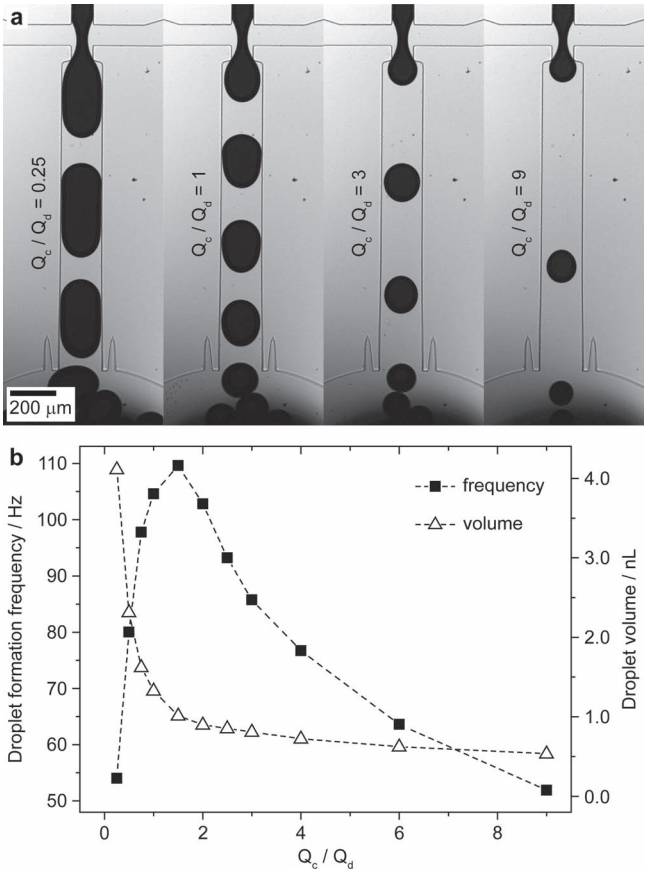

Figure 2. Liquid-metal droplet formation in aqueous PEG solution using a device with 80 µm nozzle geometry. a) Series of microscopy images depicting the droplet generation at different flow-rate ratios. b) Formation frequency and volume of liquid-metal droplets vs. flow-rate ratio Q_c/Q_d.

in **Figure 2**a. In Figure 2b, the droplet-formation frequency and droplet volume are plotted against the flow-rate ratio. Comparing these curves to the ones referring to the 40 µm nozzle (Figure 1), very similar trends can be observed, i.e., with increasing Q_c/Q_d, the volume drops sharply and the frequency rises to a maximum before it decreases again. However, the droplet-formation frequency values are considerably smaller and the droplet volumes are much bigger than for the 40 µm geometry. The highest frequency is now 110 Hz for Q_c/Q_d = 1.5 and the lowest is 52 Hz at the highest flow-rate ratio of 9. The droplet volume decreases from 4.1 nL for Q_c/Q_d = 0.25 to 0.54 nL for Q_c/Q_d = 9.

It should also be noted that the added SDS surfactant proved effective in stabilizing the water-liquid-metal interface. As for standard oil/water biphasic systems, the presence of SDS prevented the produced microdroplets from coalescing. Thus it can be assumed that the surfactant migrates to the water–liquid-metal interface, with the hydrophobic part attached to the liquid-metal surface.

2.2. Droplet Formation in Silicone Oil

In a second series of microfluidic experiments, we used silicone oil as the continuous phase. We used the same device designs as previously, with either 40 µm or 80 µm nozzle geometry. This time, the surface of the microfluidic channels was made hydrophobic prior to droplet generation using a commercial fluorosilane compound. However, in contrast to the aforementioned hydrophilic polyelectrolyte multilayer coatings, this hydrophobic treatment did not entirely prevent the channel from being stained with the metal. In the course of all metal-in-oil droplet formation experiments, we observed an increasing amount of metal being deposited onto the microchannel walls.

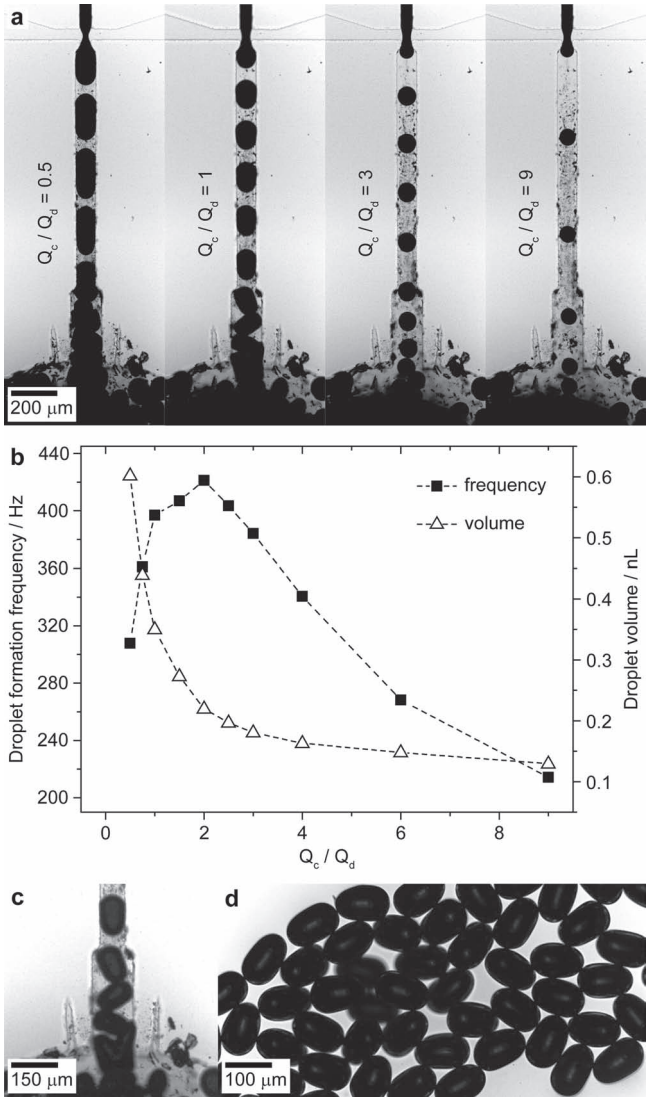

Figure 3. Liquid-metal droplet formation in oxygenated silicone oil using a device with 40 µm nozzle geometry. a) Series of microscopy images depicting the droplet generation at different flow-rate ratios. b) Formation frequency and volume of liquid-metal droplets *vs.* flow rate ratio Q_c/Q_d. c) Microscopy image of liquid-metal droplets produced at $Q_c/Q_d = 1$. They retain their non-spherical geometry when passing the channel expansion. d) Microscopy image showing non-spherical liquid-metal droplets produced at $Q_c/Q_d = 1$ on top of a glass slide.

2.2.1. Droplet Formation in 40 µm Flow-Focusing Devices

Again we kept the total flow rate to be constant - for the 40 µm nozzle at 1000 µL h^{-1} - and varied systematically the flow-rate ratio Q_c/Q_d. Microscopy images depicting the liquid-metal droplet generation with the 40 µm nozzle at different flow-rate ratios are displayed in **Figure 3**a. The droplet-formation frequency and the droplet volume are plotted against Q_c/Q_d in Figure 3b. Compared to the corresponding experiments with an aqueous carrier phase (Figure 1 and Figure 2), the droplet formation in silicone oil yielded similar volume and frequency curves. However, the droplet volumes are shifted towards distinctly lower and the frequencies towards higher values. With increasing Q_c/Q_d, the droplet volume decreases from 0.60 nL at $Q_c/Q_d = 0.5$ to 0.13 nL at $Q_c/Q_d = 9$, whereas the formation frequency peaks at 421 Hz for $Q_c/Q_d = 2$ and declines to 214 Hz at $Q_c/Q_d = 9$. Besides, it should be mentioned that by using silicone oil it was not possible to produce droplets at flow-rate ratios below 0.5.

However, the most striking difference in terms of droplet formation in silicone oil compared to aqueous PEG solution is the conservation of non-spherical droplet shapes. At flow ratios around 1, the liquid-metal droplets adopt rod-like morphologies in the narrow part of the microchannel due to the spatial confinement, and retain their geometry when passing the channel expansion and leaving the device (Figure 3c and Supporting Information, Movie M2). At higher ratios, the volume of the droplets is considerably smaller, and hence they are not constricted by the channel dimensions but show an unobstructed spherical shape. We transferred a droplet sample produced for $Q_c/Q_d = 1$ onto a glass slide for further analysis (Figure 3d). Because of the approximately square cross-section of the microchannel at the flow-focusing region, the elongated droplets are rotationally symmetric with respect to their long axis. On average, the "micro-rice" droplets exhibit a length of 113 (± 2) µm and a width of 73 (± 1) µm, yielding an aspect ratio of 1.5. It can be seen that the non-spherical shape is retained and that the EGaIn liquid metal does not reflow to minimize its surface energy. We believe that this behavior is caused by an oxide skin forming instantaneously when the liquid metal gets in contact with oxygen dissolved in the silicone oil carrier fluid. This oxide shell stabilizes non-spherical droplet geometries and prevents the droplets from deforming subsequently into spheres.

2.2.2. Droplet Formation in 80 µm Flow-Focusing Devices

When using the 80 µm nozzle, the total flow rate had to be increased to 2000 µL h^{-1} and flow-rate ratios of $Q_c/Q_d \geq 0.75$ had to be applied, since for lower values, no stable liquid-metal droplet formation was achieved. Microscopy images showing the droplet generation at selected flow-rate ratios are displayed in **Figure 4**a. As illustrated in Figure 4b, with increasing flow-rate ratio, the droplet volume drops from 1.2 nL at $Q_c/Q_d = 0.75$ to 0.37 nL at $Q_c/Q_d = 9$. The formation–frequency curve shows the usual shape, peaking at 327 Hz at $Q_c/Q_d = 1.5$ and declining to 150 Hz at $Q_c/Q_d = 9$. Due to the higher total flow rate, no direct quantitative comparison with previous experiments can be drawn at this stage.

As in the case of the 40 µm nozzle, liquid-metal droplets produced with the 80 µm device tend to retain non-spherical geometries. However, they are less rigid before leaving the microfluidic chip. In fact, when they collide at the channel expansion, they get squeezed and more elongated perpendicular to the flow direction (Figure 4c). The 80 µm droplets are considerably bigger than the 40 µm ones, and hence their surface-to-volume ratio is much smaller. This means that, assuming the oxide layer has a similar thickness in both cases, the 80 µm droplets are less stabilized by the oxide layer than the 40 µm ones, causing them to reshape on-chip.

The liquid-metal microdroplets produced in silicone oil at $Q_c/Q_d = 1$ were collected on a glass slide for imaging, and can be seen

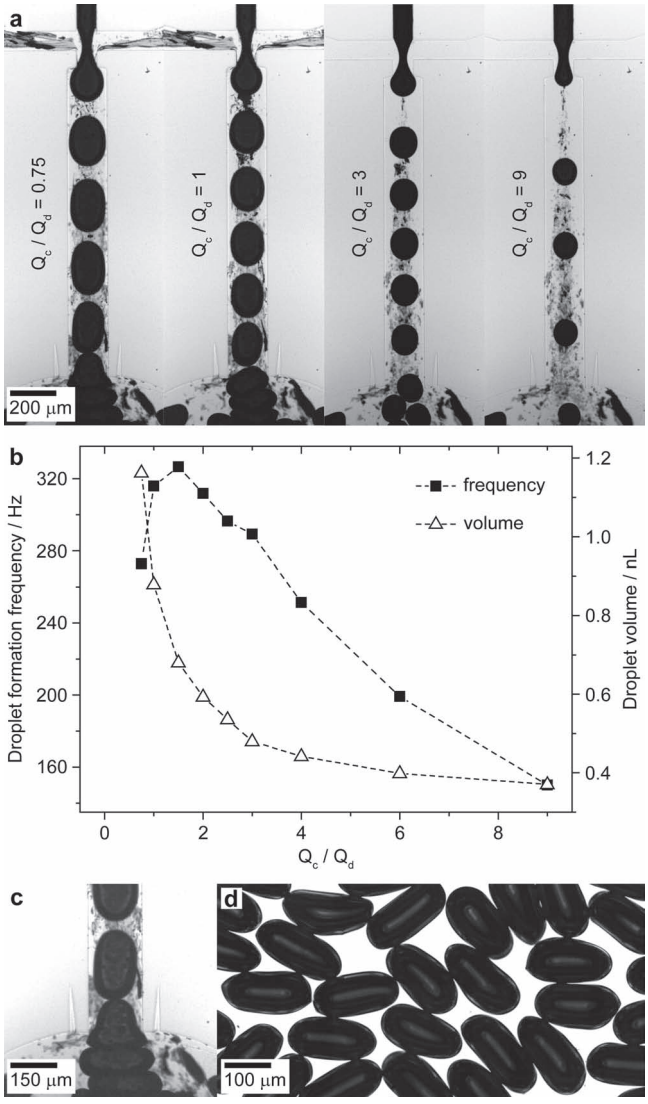

Figure 4. Liquid-metal droplet formation in oxygenated silicone oil using a device with 80 µm nozzle geometry. a) Series of microscopy images depicting the droplet generation at different flow-rate ratios. b) Formation frequency and volume of liquid-metal droplets *vs.* flow-rate ratio Q_c/Q_d. c) Microscopy image of liquid-metal droplets produced at $Q_c/Q_d = 1$. At the channel expansion, they collide and reshape. The non-spherical droplet geometry is preserved when leaving the microfluidic device. d) Microscopy image showing non-spherical liquid-metal droplets produced at $Q_c/Q_d = 1$ on top of a glass slide.

in Figure 4d. They have an average length of 181 (± 6) µm and an average width of 89 (± 2) µm, and thus an aspect ratio of 2.0. The aforementioned reshaping of these droplets on-chip apparently reduced the level of uniformity, yielding distinctly higher standard deviations, especially of the length, compared to the 40 µm case.

2.3. Additional Experimental Studies

2.3.1. Droplet Formation in Deoxygenated Silicone Oil

It is important to note that the non-spherical droplets formed in oxygenated silicone oil retained their shape and did not spontaneously reflow to form shapes of lowest interfacial energy, as do normal liquids. The non-spherical morphology is preserved, even after a few weeks of storage in a reservoir. In order to elucidate the stabilization of rod-like EGaIn liquid-metal droplets, we bubbled nitrogen through the silicone oil for about four hours before use to remove any dissolved oxygen. In this case, the droplets readily changed their shape upon passing the expansion region of the microfluidic channels, to become spherical (Supporting Information, Figure S4). Such behavior can be explained by the fact that oxygen has a distinctly higher solubility in silicone oil than in water,[36] facilitating the formation of an oxide skin, which is thick enough to be mechanically rigid so as to retain the non-spherical shape of the metal droplets. In contrast, in deoxygenated silicone oil and in aqueous PEG solution, there is not enough free oxygen to form a thick oxide skin around the droplets and therefore they reshape according to the lowest surface energy. Our findings are in good agreement with a similar observation reported in the literature. When depositing a drop of EGaIn in air from a needle onto a surface, the drop did not retract into a spherical shape, which was attributed to the formation of the oxide skin. The surface properties of oxidized EGaIn and the composition of the skin layer have been described elsewhere.[18–20] Other metals, such as pure gallium or InBiSn, that have melting points above room temperature, can be used at higher temperatures (by heating the metal and the continuous flow liquid before introduction to the microchannels) to generate droplets which then maintain their shape when cooled down to room temperature. However, using a low melting point liquid metal alloy capable of forming an oxide skin, we can easily generate permanently non-spherical liquid-metal droplets at room temperature.

2.3.2. Reduction of Liquid-Metal Droplet Size

In addition, we addressed the issue of scaling down on the liquid-metal droplet system. For various applications, it would be desirable to produce smaller droplets, and therefore we manufactured a microchannel with a minimum width of 20 µm at the nozzle and a channel height of 10 µm (Supporting Information, Figure S3). In a preliminary proof-of-principle experiment, we used the aforementioned aqueous PEG solution containing SDS as the continuous phase. Flow rates of 100 µL h-1 and 150 µL h-1 were applied for the metal and PEG solution, respectively. We successfully produced liquid-metal droplets with diameters below 30 µm (**Figure 5**). However, in order to achieve long-term stability, further optimization of the flow conditions is necessary.

2.3.3. Interfacial Tension Measurements

The interfacial tension (IFT) of the liquid-metal in the carrier fluids (aqueous PEG solution, silicone oil and deoxygenated silicone oil) was measured. We have used a needle attached to a gas-tight glass syringe to generate a metal drop in a cuvette filled with the respective continuous fluid (Supporting Information, Figure S5). The results are summarized in **Table 1**.

The values for oxygenated and deoxygenated silicone oil are practically identical, which shows that the oxide layer formed at the interface when oxygen is present only has a strong effect on

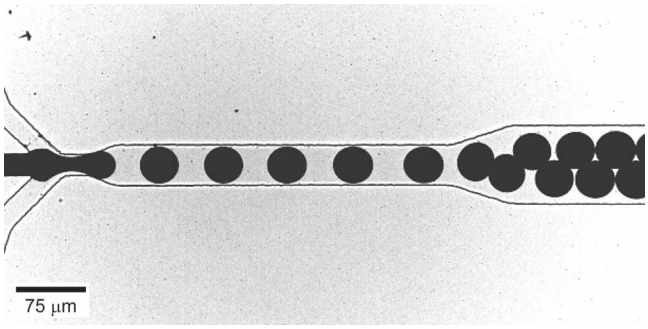

Figure 5. microscopy image showing the formation of liquid-metal droplets in aqueous PEG solution with a diameter <30 μm in a microfluidic device with a 20 μm nozzle size.

the surface properties at smaller scales, i.e., in a microfluidic setup. The interfacial tension value for the PEG solution is considerably higher than for silicone oil.

2.3.4. Viscosity Measurements

The viscosity of the silicone oil and aqueous 20% PEG + 5% SDS solution was measured to be 45.1 (± 0.3) and 92.6 (± 1.9) mPa s, respectively. Both display Newtonian behavior in the measured shear range 2–400 s^{-1} for silicone oil and 1–400 s^{-1} for aqueous 20% PEG + 5% SDS solution (Supporting Information, **Figure S6**).

Usually when dealing with biphasic systems, it is common practice to use similar viscosities of the carrier and droplet-forming liquids in order to get stable droplet formation. In our system, there is a big difference between the viscosity of the carrier fluids and the viscosity of the liquid metal (1.99 mPa s). And although the two carrier fluids–silicone oil and aqueous PEG solution–exhibit significantly different viscosities, both of them allow for the stable production of liquid-metal microdroplets for a wide range of flow-rate ratios. Comparing the interfacial tension values of aqueous PEG and silicone oil, they are not very different; thus, such a huge difference in the used viscosities may be attributed to other properties of the liquid metal, such as the density and the oxide skin.

3. Conclusions

We have shown that a liquid-metal can be used to form microdroplets in microfluidic channels. The droplets retain their non-spherical shape in oxygenated silicone oil due to the instantaneous formation of a rigid oxide skin. The proposed mechanical rigidity of the oxide skin formed on the surface of EGaIn microdroplets in oxygenated silicone oil means that, in principle, droplets having arbitrary (non-circular) cross-sections can be prepared using microchannels with a suitable geometry, which will retain their shape on egress from the channels. In aqueous solution and deoxygenated silicone oil, the metal droplets behave like any normal liquid, *i.e.* they minimize the surface energy by adopting a spherical geometry. As in other biphasic systems, adding surfactants prevents the liquid-metal droplets from coalescing. Applying systematic variations of the flow-rate ratios, we demonstrated that our metal-in-water and metal-in-oil systems behave in a very cohesive and reliable way in terms of droplet volume and droplet-formation frequency. This proves the high level of control and reproducibility offered by our microfluidic approach. The size of the microdroplets was decreased to <30 μm diameter, and can potentially be further scaled down by using smaller microchannels. We believe that the liquid-metal droplet system we introduce here has great potential for applications in microfluidics, electronics and optics.

Table 1. Interfacial tension measurement results.

Carrier Fluid	IFT [mN m^{-1}]	Average drop volume [μm]
Silicone oil	90 (± 2)	15.0 (± 0.4)
Silicone oil, deoxygenated	89 (± 2)	14.8 ± (0.3)
Aqueous 20 wt% PEG, 5 wt% SDS	101 (± 2)	15.2 ± (0.4)

4. Experimental Section

Unless stated otherwise, all chemicals were obtained from Sigma-Aldrich and used as received without further purification. Milli-Q water (Millipore) was used throughout all of the experiments. Silicone oil was purchased from Breckland Scientific suppliers.

EGaIn Preparation: Pure indium with ≥99.9% purity was used. Pure gallium was purchased from Alfa Aesar with 99.999% purity. The eutectic concentration was achieved by taking the weight of each metal in the ratio of 75.5 wt% gallium and 24.5 wt% indium. The metals were placed in a vial and heated for half an hour on a hot plate, then mixed with a glass pipette.

Preparation of the Aqueous PEG Solution: PEG with an average molecular weight of ~20 000 was used. An aqueous solution of 20 wt% PEG and 5 wt% SDS in Milli-Q water was prepared by mixing and shaking, and left overnight to dissolve completely.

Microfluidic Device Fabrication: Microfluidic devices were produced by conventional soft lithographic techniques.[37,38] Microchannels were designed with AutoCAD (AutoDesk) and transferred to high-resolution photomasks fabricated on transparencies (Circuit Graphics). The negative photoresist SU-8 2025 (MicroChem) was spin-coated onto 3 inch silicon wafers (Compart Technology) and patterned using a MJB4 mask aligner (Süss MicroTec). Development was accomplished by immersion into 1-methoxy-2-propyl acetate.

A commercially available Sylgard 184 PDMS kit (Dow Corning), containing the pre-polymer and a cross-linker, was used in the recommended ratio of 10: 1 (w/w). The mixture was poured on top of the patterned silicon wafers and degassed. After curing at 80 °C for 10 h, the PDMS cast was cut and peeled off the wafers. Inlets and outlets were stamped out using a biopsy punch (Kai Industries) with an outer diameter of 1 mm. The microfluidic devices were assembled by joining the PDMS cast and a microscope glass slide. Bonding strength was provided by pre-treating both contact surfaces with an oxygen plasma for 8 s in a Femto plasma cleaner (Diener electronic). Storage devices were fabricated following the same process. Instead of patterned wafers, microscope cover slips glued onto glass slides were used as casting molds.

Surface Modification of the Microchannels: Hydrophilic surface properties were obtained by deposition of a polyelectrolyte multilayer onto the microchannel walls. The details of our layer-by-layer surface-modification method are described elsewhere.[35] Solutions of NaCl

(AnalaR) in water (0.1 M), as well as of poly(allylamine hydrochloride) (M_w ~56 000) and poly(sodium 4-styrenesulfonate) (M_w ~70 000), both 0.1 wt% in 0.5 M aqueous NaCl solution, were prepared. Segments of these solutions, separated by air plugs, were loaded into a piece of polyethylene (PE) tubing (Becton Dickinson) with an inner diameter of 380 µm. Using a PHD 2000 syringe pump (Harvard Apparatus), they were sequentially flushed through the microchannel at a constant flow rate of 50 µL h^{-1}. Hydrophobic (fluorophilic) channel surfaces were produced by flushing the microchannels for 5 min with the commercially available water-repellent agent Aquapel (PPG Industries).

Microfluidic Experiments: Two different continuous fluid phases were used: (i) water containing 20 wt% PEG (M_w ~20 000) and 5 wt% SDS, and (ii) silicone oil (Breckland Scientific Supplies). Depletion of the dissolved oxygen in the silicone oil was achieved by streaming nitrogen gas through the liquid for 5 h.

EGaIn, and the carrier fluids silicone oil or the aqueous PEG/SDS solution, were injected into microfluidic devices via PE tubes (Becton Dickinson). In all microfluidic experiments, PHD 2000 syringe pumps (Harvard Apparatus) were used to stream liquids at constant flow rates, between 100 µL h^{-1} and 1800 µL h^{-1}, through the microchannels. The EGaIn did not stain the PE tubing nor the channels, and only slightly in the case of the silicone oil measurements. Owing to its very low viscosity, it was easy to handle. The estimated values for viscosity of EGaIn are $1.99 * 10^{-3}$ Pa s for the dynamic viscosity and $3.2 * 10^{-7}$ m^2 s^{-1} for the kinematic viscosity, from previos works.[39]

Droplet formation on-chip as well as emulsion samples inside storage devices were imaged using a monochromatic Phantom v7.2 camera (Vision Research) attached to an IX71 inverted microscope (Olympus). Droplet formation frequencies were calculated by analyzing high-speed movies with Phantom Camera Control Version 8.4 (Vision Research) software. The time needed for the formation of 20 droplets was determined and converted into the formation frequency. Diameter distributions of spherical droplets were obtained by measuring the diameter of 100 droplets in a reservoir. Non-spherical droplets were analyzed on glass slides, *i.e.* the long and the short axes of 20 droplets were measured and the average length and width, as well as the aspect ratio, were calculated. The size analysis of spherical and non-spherical droplets was conducted using ImageJ 1.44 (National Institutes of Health) software.

Viscosity Measurements: Viscosity measurements were performed at 25 °C using an ARES control strain rheometer (from Rheometric Scientific) with a 50 mm diameter parallel-plate geometry, fitted with a water-bath temperature controller, ± 1 °C. The aqueous solution was measured with a humidity cover to prevent water evaporation during the measurement.

Interfacial Tension Measurements: A FTA1000 instrument (Firsttenangtroms) with dedicated FTA software was used for the IFT measurements of EGaIn liquid metal in aqueous PEG solution, silicone oil and deoxygenated silicone oil. A 100 µL glass syringe equipped with a stainless steel needle and filled with EGaIn was placed above a cuvette containing the desired liquid, and a measurement was performed on a pendant drop of EGaIn. Droplets were extruded into the tested liquid at a flow rate of 0.3 µL s^{-1} until a volume of ~15 µL was obtained. A snapshot was taken and the IFT was calculated over the droplet curvature with a Laplace-Young fit.

Supporting Information

Supporting Information is available from the Wiley Online Library or from the authors.

Acknowledgements

The authors T.H. and W.-A.C.B. contributed equally to this work. The authors gratefully acknowledge the assistance of Xin Liu and Gesine Gunkel in terms of device fabrication and IFT measurements, respectively. This work was supported by the EPSRC, the RCUK Basic Technology Programme, Fonds der Chemischen Industrie and the Cambridge European Trusts. T. Hutter acknowledges a studentship from Trinity College, Cambridge.

Note added in proof: During publishing, we became aware of a powerful application for GaIn liquid microdroplets in the autonomic restoration of electrical conductivity.[40]

Received: February 2, 2012
Published online: March 21, 2012

[1] G. M. Whitesides, *Nature* **2006**, *442*, 368.
[2] A. B. Theberge, F. Courtois, Y. Schaerli, M. Fischlechner, C. Abell, F. Hollfelder, W. T. S. Huck, *Angew. Chem. Int. Ed.* **2010**, *49*, 5846.
[3] B. Kintses, L. D. van Vliet, S. R. A. Devenish, F. Hollfelder, *Curr. Opin. Chem. Biol.* **2010**, *14*, 548.
[4] P. B. Umbanhowar, V. Prasad, D. A. Weitz, *Langmuir* **1999**, *16*, 347.
[5] S.-Y. Park, T.-H. Wu, Y. Chen, M. A. Teitell, P.-Y. Chiou, *Lab Chip* **2011**, *11*, 1010.
[6] D. R. Link, E. Grasland-Mongrain, A. Duri, F. Sarrazin, Z. Cheng, G. Cristobal, M. Marquez, D. A. Weitz, *Angew. Chem. Int. Ed.* **2006**, *45*, 2556.
[7] L. M. Fidalgo, C. Abell, W. T. S. Huck, *Lab Chip* **2007**, *7*, 984.
[8] D. R. Link, S. L. Anna, D. A. Weitz, H. A. Stone, *Phys. Rev. Lett.* **2004**, *92*, 054503.
[9] Y.-C. Tan, J. S. Fisher, A. I. Lee, V. Cristini, A. P. Lee, *Lab Chip* **2004**, *4*, 292.
[10] L. M. Fidalgo, G. Whyte, B. T. Ruotolo, J. L. P. Benesch, F. Stengel, C. Abell, C. V. Robinson, W. T. S. Huck, *Angew. Chem. Int. Ed.* **2009**, *48*, 3665.
[11] J.-u. Shim, L. F. Olguin, G. Whyte, D. Scott, A. Babtie, C. Abell, W. T. S. Huck, F. Hollfelder, *J. Am. Chem. Soc.* **2009**, *131*, 15251.
[12] W.-A. C. Bauer, J. Kotar, P. Cicuta, R. T. Woodward, J. V. M. Weaver, W. T. S. Huck, *Soft Matter* **2011**, *7*, 4214.
[13] X.-s. Zhu, C. Gao, J.-W. Choi, P. L. Bishop, C. H. Ahn, *Lab Chip* **2005**, *5*, 212.
[14] J.-H. So, M. D. Dickey, *Lab Chip* **2011**, *11*, 905.
[15] A. C. Siegel, D. A. Bruzewicz, D. B. Weibel, G. M. Whitesides, *Adv. Mater.* **2007**, *19*, 727.
[16] A. C. Siegel, S. K. Y. Tang, C. A. Nijhuis, M. Hashimoto, S. T. Phillips, M. D. Dickey, G. M. Whitesides, *Accounts Chem. Res.* **2010**, *43*, 518.
[17] S. Xu, Z. Nie, M. Seo, P. Lewis, E. Kumacheva, H. A. Stone, P. Garstecki, D. B. Weibel, I. Gitlin, G. M. Whitesides, *Angew. Chem. Int. Ed.* **2005**, *44*, 724.
[18] M. D. Dickey, R. C. Chiechi, R. J. Larsen, E. A. Weiss, D. A. Weitz, G. M. Whitesides, *Adv. Funct. Mater.* **2008**, *18*, 1097.
[19] R. C. Chiechi, E. A. Weiss, M. D. Dickey, G. M. Whitesides, *Angew. Chem. Int. Ed.* **2008**, *47*, 142.
[20] R. J. Larsen, M. D. Dickey, G. M. Whitesides, D. A. Weitz, *J. Rheol.* **2009**, *53*, 1305.
[21] Y.-L. Park, C. Majidi, R. Kramer, P. Bérard, R. J. Wood, *J. Micromech. Microeng.* **2010**, *20*, 125029.
[22] T. S. Kasirga, Y. N. Ertas, M. Bayindir, *Appl. Phys. Lett.* **2009**, *95*, 214102.
[23] S. Cheng, A. Rydberg, K. Hjort, Z. Wu, *Appl. Phys. Lett.* **2009**, *94*, 144103.
[24] C. Shi, W. Zhigang, P. Hallbjorner, K. Hjort, A. Rydberg, *IEEE T. Antenn. Propag.* **2009**, *57*, 3765.
[25] S. Cheng, Z. Wu, *Lab Chip* **2010**, *10*, 3227.
[26] J.-H. So, J. Thelen, A. Qusba, G. J. Hayes, G. Lazzi, M. D. Dickey, *Adv. Funct. Mater.* **2009**, *19*, 3632.

[27] M. Kubo, X. Li, C. Kim, M. Hashimoto, B. J. Wiley, D. Ham, G. M. Whitesides, *Adv. Mater.* **2010**, *22*, 2749.
[28] J. Q. Yu, Y. Yang, A. Q. Liu, L. K. Chin, X. M. Zhang, *Opt. Lett.* **2010**, *35*, 1890.
[29] M. Hashimoto, B. Mayers, P. Garstecki, G. M. Whitesides, *Small* **2006**, *2*, 1292.
[30] L. Junghoon, K. Chang-Jin, *J. Microelectromech. Syst.* **2000**, *9*, 171.
[31] P. Sen, K. Chang-Jin, *IEEE T. Ind. Electron.* **2009**, *56*, 1314.
[32] J. T. H. Tsai, C.-M. Ho, F.-C. Wang, C.-T. Liang, *Appl. Phys. Lett.* **2009**, *95*, 251110.
[33] J. Simon, S. Saffer, C.-J. Kim, *J. Microelectromech. Syst.* **1997**, *6*, 208.
[34] J. Simon, S. Saffer, F. Sherman, K. Chang-Jin, *IEEE T. Ind. Electron.* **1998**, *45*, 854.
[35] W.-A. C. Bauer, M. Fischlechner, C. Abell, W. T. S. Huck, *Lab Chip* **2010**, *10*, 1814.
[36] F. Jakob, K. Jakob, N. Perjanik, in Silicone Dielectric Fluids, Analytical ChemTech International Inc., Saint Johnsbury, VT, USA: http://www.weidmann-solutions.cn/zhenduan/silicone_dielectric_fluids.pdf (accessed March, 2012).
[37] D. Qin, Y. Xia, G. M. Whitesides, *Adv. Mater.* **1996**, *8*, 917.
[38] D. C. Duffy, J. C. McDonald, O. J. A. Schueller, G. M. Whitesides, *Anal. Chem.* **1998**, *70*, 4974.
[39] J. N. Koster, R. Derebail, A. Grötzbach, *Appl. Phys. A–Mater.* **1997**, *64*, 45.
[40] B.J. Blaiszik, S. L. B. Kramer, M. E. Grady, D. A. McIllroy, J. S. Moore, N. R. Sottos, S. R. White, *Adv. Mater.* **2012**, *24*, 398.